Journal of Fluorescence, Vol. 15, No. 3, May 2005 (© 2005)
DOI: 10.1007/s10895-005-2635-y

Concept for the Traceability of Fluorescence (Beads) in Flow Cytometry: Exploiting Saturation and Microscopic Single Molecule Bleaching

Jörg Neukammer,[1,5] Carsten Gohlke,[1,2] Benedikt Krämer,[1,3] and Martin Roos[4]

Received January 28, 2005; accepted December 6 2004

We have determined the fluorescence yield of stained micro beads, used for calibration purposes in flow cytometry, as function of the irradiance of the exciting laser beam. A rate equation model has been applied to derive the number of fluorescence molecules carried by each micro bead. To derive *in situ* photo-physical properties of the specific dye, required for the rate equation model, we discuss an approach based on flow cytometric sorting of micro beads, which have passed two laser beams with properly chosen different irradiances, and subsequent observation of single molecule bleaching employing high sensitivity microscopy. The feasibility of our approach is demonstrated presenting first results concerning saturation of fluorescence of beads in flow and single molecule bleaching by high sensitivity microscopy.

KEY WORDS: Flow cytometry; MESF; quantification of fluorescence; saturation of laser induced fluorescence; single molecule bleaching.

INTRODUCTION

Flow cytometry [1–6] is a technique routinely used in different fields of medicine to differentiate human cells in blood samples, sputum, bone marrow, liquor, and cells isolated from biopsies. Cell differentiation is accomplished by impedance changes, light scatter and laser induced fluorescence. The main advantage of flow cytometry is the analysis of cells, passing a corresponding interaction region in single file, at high throughput and the possibility to sort cells, e.g. for subsequent microscopic investigations or to enrich rare cells.

In particular, flow cytometric detection of blood cells, stained with fluorescently labeled monoclonal antibodies is routinely used to support medical diagnoses of various (hematological) malignancies including leukemia [7–9] and HIV diagnosis [10]. Moreover, flow cytometry is a powerful tool in clinical and basic research, e.g. to detect minimal residual disease in leukemia [11] or to characterize antigen-specific lymphocytes [12]. Generally, for most applications identification of positive target cells is required, the measurand used for medical diagnosis being the concentration of these cells or relative concentrations. To give an example, for HIV diagnosis the ratio between CD4 positive T helper cells and CD8 positive lymphocytes is measured. For this purpose, the determination of relative fluorescence intensities is sufficient. However, quantification of the number of specific proteins on cell surfaces, the so-called antibody binding capacity (ABC), is expected to be a valuable tool to monitor cell activation, induced for example by cell–cell interaction. Recently, a study including the determination of ABC has been performed aiming at the prediction of infections in risk patients [13] resulting in immune paralysis or sepsis. As an

[1] Physikalisch-Technische Bundesanstalt (PTB), Working Group 8.32, Berlin, Germany.
[2] Present address: LINOS Photonics SARL, Avenue de Lanessan 90, F - 69410 Champagne au Mont d'Or, France.
[3] Present address: PicoQuant GmbH, Rudower Chaussee 29, 12489 Berlin, Germany.
[4] Robert-Koch Institut, Nordufer 20, 13353 Berlin, Germany.
[5] To whom correspondence should be addressed. E-mail: joerg.neukammer@ptb.de

indicator, the binding capacity of monocytes with respect to antibodies against human leukocyte antigens (HLA-DR) surface proteins was studied using QuantiBRITE™ particles for calibration [14]. Besides this calibration procedure microbead kits "Quantum Simply Cellular" are available (Sigma-Aldrich, Inc.), which allow to obtain information on the antibody binding capacity of cells. Furthermore, the expression of enhanced green fluorescent protein (EGFP) on transfected T-cells was derived [15] by comparing fluorescence intensities of these cells to the fluorescence intensity of beads, validated in units of molecules of equivalent soluble fluorochrome (MESF). Apart from these two challenging applications to quantify biological characteristics, MESF beads [16]—stained with one or several selected fluorophores—are applied frequently for a day to day control as well as for a comparison of results obtained with different instruments. However, MESF units do not reflect the true number of molecules, since the absorption coefficient, the fluorescence quantum yield, the absorption and emission spectrum may change upon binding to the microparticles. Furthermore, photophysical properties are influenced by the environment to which the dye is exposed, e.g. by pH value and oxygen concentration.

To account for the changes of photo-physical properties of fluorescent dyes upon binding to e.g. antibodies and due to influences of the micro-environment, measuring techniques are required, which allow to determine these quantities *in situ*. In the following, we present first results exploiting the saturation of laser induced fluorescence for flow cytometric quantification of the number of fluorophores bound to a micro bead. To this end, we analyzed the observed saturation of the fluorescence intensity by a simple rate equation model. As one possible way to determine photo-physical quantities of fluorochromes in the environment characteristic for biological applications, we demonstrate microscopic single molecule bleaching of Alexa 647 coupled to immobilized streptavidin molecules.

EXPERIMENTAL

Flow cytometric investigations were carried out on an instrument developed at the Physikalisch-Technische Bundesanstalt [17] and used to determine reference values for round robin experiments of the complete blood count. As illustrated in Fig. 1, blood cells are classified according to their intensity of scattered light in forward and orthogonal direction and with respect to their fluorescence intensity. The flow cytometer is equipped with an Ar^+-laser (Innova 304, Coherent, USA), a Kr^+-laser and a HeNe laser (Model 106-1, Spectra Physics, USA), operated at wavelength of 488 nm, 413 nm and 633 nm, respectively. The laser beams are oriented perpendicularly to the flow cell (Hellma GmbH, Germany) with a rectangular cross-section cross-section of 8 mm × 2 mm, a length of 30 mm, and a 250 μm × 250 μm flow channel. The outer dimensions of the flow cell were chosen to

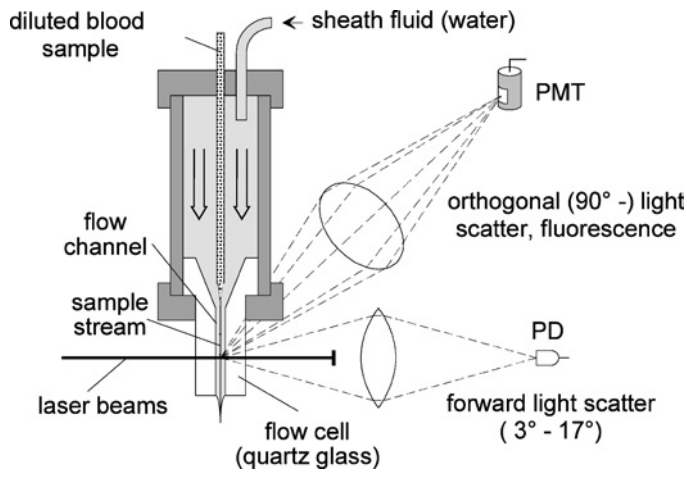

Fig. 1. Schematic representation of the essential components for flow cytometric investigation of microparticles of artificial or biological origin. The sample, e.g. diluted blood, is injected through a capillary into a quartz glass low cell. A second, sheath fluid, is used for hydrodynamic focusing of the sample stream. Single particles are classified according to their (forward, orthogonal) light scatter at different wavelengths and their laser-induced fluorescence.

allow adaptation of a condenser (63×, NA 1.4, Carl Zeiss AG, Göttingen, Germany), the diameter of the entrance lens and the cover glass correction being 8 mm and 1 mm, respectively. Because of the large numerical aperture orthogonal light scatter as well as laser induced fluorescence is observed with high efficiency, the half opening angle is determined to be 68° by ray tracing. For simultaneous detection of forward light scatter, we have used a 20×/0.40 objecive (Leitz GmbH, Wetzlar, Germany). The direct laser beam is eliminated by a circular beam stop which restricts the measurement of forward scattered light to angles larger than 3.3°. The upper limit amounts to 17.4° and follows from the specifications of the 20× objective. Fluorescence light is detected by a R2949 photomultiplier tube (Hamamatsu, Herrsching, Germany), for forward light a tube R931 with lower sensitivity is used. When observing the fluorescence of fluorescein (FITC), a band pass filter with a center wavelength of 535 nm and a full width at half maximum of 35 nm (535DF35, Omega Optical, Inc., Brattleboro, VT, USA) and a notch filter (Kaiser Optica Systems, Inc., Ann Arbor, MI, USA) to block the scattered light of the 488 nm line of the Ar^+ laser are applied. For simultaneous measurement of orthogonal light scatter at 488 nm and FITC-fluorescence, a dichroic beam splitter (505DR, Omega Optical, Inc.) was inserted in the optical path.

For microscopic investigations, we have employed a microscope stand Axiovert 35M (Zeiss AG, Göttingen, Germany), supplemented to allow confocal imaging. To achieve the high sensitivity for single molecule detection by means of fluorescence measurements, an avalanche photodiode (SPCM-AQR-14, Perkin Elmer, Inc., Santa Clara, CA, USA) was used in combination with single photon counting electronics. Fluorescence was excited by a 633 nm HeNe laser (Model 1137P, JDS Uniphase Corp., San Jose, CA, USA), focused by a 63× water immersion objective (63×, NA 1.2, Apochromat, Carl Zeiss AG, Göttingen, Germany) to a diffraction limited spot. To control photobleaching of fluorophores, the output power of the HeNe laser was adjusted by an acusto optical modulator (AA.MP.25, AA Opto-Electronic, St-Rémy-Lès-Chevreuse, France) between 0.1 μW and 10 μW, measured at the sample. Fluorescence light was collected by the same microscope objective and separated from the exciting laser beam by a triple-band beam splitter (Chroma Technology Corp., Brattleboro, VT, USA), transmitted through the confocal aperture and focused on the avalanche photodiode. Images are recorded using two movable mirrors mounted on galvanometer scanners (Model G120DT, GSI Lumonics, Munich, Germany). To observe Alexa 647 (Molecular Probes, Inc., Eugene, OR, USA) emission, a band pass (670 nm ± 20 nm) is mounted in front of the detector. It should be noted, that presently the microscopic setup allows to excite fluorophores at a 633 nm and to detect its emission between 640 nm and 700 nm. Therefore, in the context discussed in this contribution confocal microscopy is merely used to demonstrate stepwise single molecule bleaching and to show, that it is suited to determine photophysical properties of chromophores *in situ*.

RESULTS AND DISCUSSION

Observation of Fluorescence Saturation and Analysis by Rate Equations

To investigate the influence of the irradiance of the exciting laser beam on the observed fluorescence signal we have chosen mondisperse polystyrene micro beads (Polyscience, Inc., Warrington, PA, USA) with a diameter of 6.1 μm. The power of the argon ion laser, operated at a wavelength of 488 nm, was increased up to 150 mW. The power was measured directly in front of the flow cell, to obtain the power within the cell a reflection loss of 4% at the glass surface of the cell was considered. The result is shown in Fig. 2, where we have plotted the output voltage of the photomultiplier tube used to detect the laser induced fluorescence of the polystyrene microspheres versus the excitation power. Experimental values are represented by filled squares and were obtained from the maximum of the pulses recorded at a sampling rate of 1 GHz by a digital oscilloscope (DSA 602A, Tektronix GmbH, Köln, Germany) and averaged for typically 1000 signals. The uncertainty was estimated from the fluctuation of the signal heights when analyzing a smaller number of polystyrene microspheres. The line included in the figure was calculated by the rate equation model presented below.

To analyze the observed behavior of the fluorescence when increasing the laser power, the number of photons absorbed by the particles when crossing the laser beam has to be known. For this purpose we start with the well know Lambert-Beer law

$$I = I_{\mathrm{inc}} \times 10^{(-\varepsilon_{\mathrm{mol}} c z)} \tag{1}$$

and use the linear approximation

$$I \approx I_{\mathrm{inc}}(1 - \varepsilon_{\mathrm{mol}} c z \ \ln 10) \tag{2}$$

for the following discussion, since $\varepsilon_{\mathrm{mol}} c z \ll 1$ holds. The symbol I_{inc} represents the irradiance of the incident laser beam, I the irradiance after passing the sample, $\varepsilon_{\mathrm{mol}}$ the molar extinction coefficient with respect to the basis 10, c the concentration of the dye and z the thickness of the

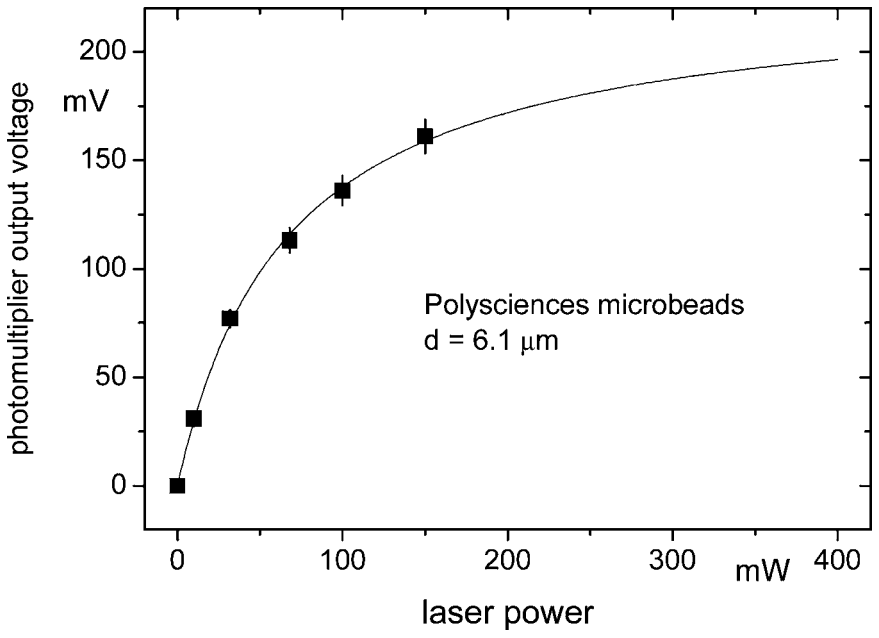

Fig. 2. Fluorescence intensity of FITC stained monodisperse polystyrene microspheres as function of the power of the exciting laser beam. The abscissa corresponds to the signal voltage of the photomultiplier tube at 50 Ω, which is proportional to the to the number of fluorescence photons emitted by the microspheres. Measured values are indicated as squares. Analysis of experimental data by fitting according to Equation (16) yields 29000 molecules for each microsphere.

sample. Generally, in flow cytometry the pulse height of the fluorescence signals is measured. The maximum of the fluorescence is reached, when the sphere is located in the center of the laser beam. Hence, the power W_{inc} incident on the sphere with diameter d is obtained by integrating the Gaussian profile

$$I_{\text{inc}} = \left(2W_{\text{inc}}/\pi w_0^2\right) \exp\left(-2R^2/w_0^2\right) \tag{3}$$

of the laser beam with diameter $2w_0$ ($1/e^2$-points) for radii $0 \leq R \leq (d/2)$. Rewriting Equation (2) as

$$W = W_{\text{inc}}(1 - \varepsilon_{\text{mol}} cz \ \ln\ 10) \tag{4}$$

and inserting the result of the integration we obtain

$$(W_{\text{inc}} - W) = N_{\text{abs}} h\nu = W_{\text{laser}} \left[1 - \exp\left\{-2\frac{(d/2)^2}{w_0^2}\right\}\right] \times (\varepsilon_{\text{mol}} cz \ \ln\ 10), \tag{5}$$

W being the power transmitted by the particle. The power $(W_{\text{inc}} - W)$ absorbed by the sphere is proportional to the product of the photon absorption rate N_{abs} and the photon energy $h\nu$, W_{laser} denotes the total power of the laser beam. Finally, by introducing the quantum efficiency Q_{fl}, the rate of fluorescence photons emitted into the total solid angle is determined according to

$$N_{\text{fl}} = Q_{\text{fl}} N_{\text{abs}} = Q_{\text{fl}} \frac{W_{\text{Laser}} \left[1 - \exp\left\{-2\frac{(d/2)^2}{w_0^2}\right\}\right]}{h\nu} \times (\varepsilon_{\text{mol}} cz \ \ln\ 10). \tag{6}$$

Different absorption path lengths of rays passing the sphere and scattering losses are not considered. This approach corresponds to an approximation of the sphere as volume equivalent cylinder with its base area identical to the sphere's cross-section and oriented perpendicular to the laser beam. Consequently, the height of the cylinder is interpreted as absorption length z.

To justify the linear approximation of Lambert-Beer's law, we calculate the quantity $\varepsilon_{\text{mol}} cz$ using the molar extinction coefficient of FITC $\varepsilon_{\text{mol}} = 8 \times 10^4$ l/mol cm [18, 19] at a wavelength $\lambda = 488$ nm for a particle of diameter $d = 6.1\,\mu$m. Assuming a particle stained with 10000 molecules, we obtain $\varepsilon_{\text{mol}} cz = 4.545 \times 10^{-6}$, for 5×10^6 fluorochromes per particle $\varepsilon_{\text{mol}} cz$ amounts to 2.273×10^{-3} proving the validity of our assumption in Equation (1). It should be noted, that the number of surface epitopes of cells will generally not exceed 10^6. Hence, the number of fluorochromes on cell surfaces will not be

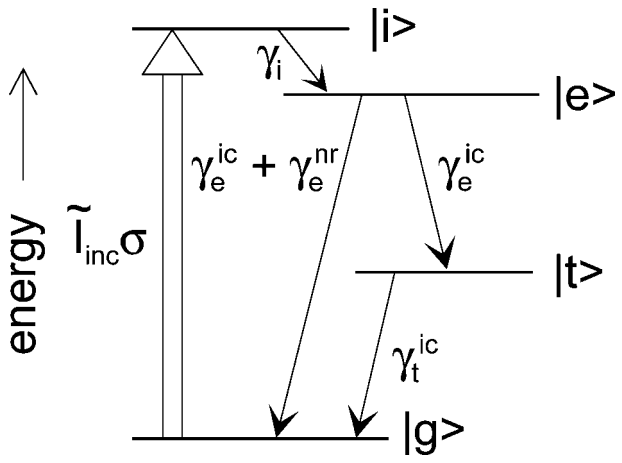

Fig. 3. Term scheme to explain the saturation of the fluorescence of stained microspheres. The relevant energy levels are labeled $|g\rangle$, $|i\rangle$, $|e\rangle$, and $|t\rangle$ for the ground state, the intermediate state, the excited and the triplet state. For the excitation rate and for the various relaxation rates we use the notations $\tilde{I}_{inc}\sigma$ and γ, respectively.

larger then about 5×10^6 taking an average load of 5 fluorescence molecules per antibody.

We have calculated the emission rate of fluorescence photons from Equation (6) using the value $2w_0 = 10\,\mu$m for the beam waist of the laser and a power of 100 mW, which corresponds to the experimental conditions in our experiment. It follows, that each molecule emits $N_{fl} \approx 1 \times 10^8$ photons, the average time between two successive emissions being approximately 10 ns. Since this time exceeds the fluorescence lifetime of FITC, which is 4.5 ns [19], only by a factor of 2, saturation effects must be taken into account.

The term scheme used for the rate equation model is depicted in Fig. 3. The fluorescent molecules, characterized by the absorption cross-section σ, are excited from the ground state $|g\rangle$ to the intermediate state $|i\rangle$ by absorbing photons from the incident laser beam. The photon flux density of the laser beam is given by $\tilde{I}_{inc}$. From the intermediate state $|i\rangle$ the molecules quickly pass to the excited level $|e\rangle$ by nonradiative transitions, subsequently they decay directly or via the triplet state $|t\rangle$ in the ground state $|g\rangle$. The temporal change of the population of each state is given by the rate equations

$$\begin{aligned}
\frac{\mathrm{d}}{\mathrm{d}t}n_g &= \gamma^{tr}\left(n_g^0 - n_g\right) - \tilde{I}_{inc}\sigma n_g + \left(\gamma_e^{fl} + \gamma_e^{nr}\right)n_e + \gamma_t^{ic} n_t \\
\frac{\mathrm{d}}{\mathrm{d}t}n_e &= \gamma^{tr}(-n_e) + \tilde{I}_{inc}\sigma n_g - \left(\gamma_e^{fl} + \gamma_e^{nr} + \gamma_e^{ic}\right)n_e \qquad (7) \\
\frac{\mathrm{d}}{\mathrm{d}t}n_t &= \gamma^{tr}(-n_t) + \gamma_e^{ic} n_e - \gamma_t^{ic} n_t.
\end{aligned}$$

with n_g, n_e, and n_t representing the population of molecules in the ground state, excited state and triplet state. All molecules enter the laser beam in the ground state at a rate $\gamma^{tr} n_g^0$ determined by the transit time, the upper index 0 indicating time zero. In addition, the transit of the molecules through the laser beam results in a loss of molecules in each of the states, described by the terms $-\gamma^{tr} n_g$, $-\gamma^{tr} n_e$, and $-\gamma^{tr} n_t$. The relaxation rates γ_e^{fl}, γ_e^{nr}, and γ_e^{ic} account for the decay of the excited state into the ground state by fluorescence radiation or nonradiative transition and for the intersystem crossing in the triplet system. The population of the excited level takes place via the intermediate level. However, the corresponding number n_i does not enter the rate equations, since the relaxation rate γ_i significantly exceeds all other rates. Vibrational-rotational coupling of the intermediate and excited states results in relaxation times in the ps region, while the lifetime of the excited level is several ns. Furthermore, because of the high relaxation rate γ_i stimulated emission $|i\rangle \rightarrow |g\rangle$ is negligible. It follows, that direct occupation of the excited level is accounted for by the term $\tilde{I}_{inc}\sigma n_g$ and the term describing the stimulated emission $-\tilde{I}_{inc}\sigma n_e$ does not enter the rate equations. It should be noted, that the sum $n_g + n_e + n_t = n_g^0$ is constant, i.e. other mechanisms which might influence the population of these molecular levels, are not included in the model. In particular, photodissociation of the excited level $|e\rangle$, which is important for microscopic investigations [20] is not relevant when describing saturation in flow cytometry because of the short interaction time of stained particles with the exciting laser beam. The stationary solution of the rate equations, i.e. $(\mathrm{d}n_g/\mathrm{d}t) = (\mathrm{d}n_e/\mathrm{d}t) = (\mathrm{d}n_t/\mathrm{d}t) = 0/s$ is given by

$$n_e = \frac{\tilde{I}_{inc}\sigma}{\gamma_e} n_g^0 \Bigg/ \left\{1 + \frac{\tilde{I}_{inc}\sigma}{\gamma_e}\left(1 + \frac{\gamma_e^{ic}}{\gamma^{tr} + \gamma_t^{ic}}\right)\right\}, \qquad (8)$$

where we have used the abbreviation $\gamma_e = \gamma^{tr} + \gamma_e^{fl} + \gamma_e^{nr} + \gamma_e^{ic}$. The photon flux density $\tilde{I}_{inc}$ has to be replaced by the average photon flux density

$$\langle \tilde{I}_{inc} \rangle = \frac{\langle \tilde{I}_{inc} \rangle}{h\nu} = \frac{W_{inc}}{h\nu\pi(d/2)^2}, \qquad (9)$$

which is related to the laser power W_{laser} corresponding to Equation (5) according to

$$\langle \tilde{I}_{inc} \rangle = \frac{W_{laser}\left[1 - \exp\left\{-2\frac{(d/2)^2}{w_0^2}\right\}\right]}{h\nu\pi(d/2)^2}. \qquad (10)$$

The fluorescence signal observed and therefore the output voltage U of the photomultiplier tube, measured at the input resistor of the data acquisition system, is proportional to the number of molecules n_e occupying the

excited state

$$U = P_0 Q_{\mathrm{fl}} n_{\mathrm{e}} \gamma_{\mathrm{e}}. \tag{11}$$

Using Equation (8) which describes the population n_e, the signal voltage as function of the laser power is given by the relation

$$U = \frac{P_1 W_{\mathrm{Laser}}}{1 + P_2 W_{\mathrm{Laser}}}. \tag{12}$$

The factor P_0 appearing in Equation (11) has the dimension $[P_0] = Vs$ and is determined by the characteristics of the different components of the flow cytometer. In particular, the solid angle $\Delta\Omega$ and the transmission $T_{\mathrm{objective}}$ of the (microscope) objective used to observe the fluorescence, the transmission of bandpass filters T_{filter}, the quantum efficiency $Q_{\mathrm{photocathode}}$ of the photomultipliers photocathode and its current gain G, the elementary charge e_0 and the load resistance $R_{\mathrm{load}} = 50\,\Omega$ of the data acquisition system used for pulse height analysis have to be considered

$$P_0 = \Delta\Omega T_{\mathrm{objective}} T_{\mathrm{filter}} Q_{\mathrm{photocathode}} e_0 G R_{\mathrm{load}}. \tag{13}$$

The relation between the parameters P_1, P_2 and the quantities introduced before is obtained by inserting the results for n_{e} and $\langle \tilde{I}_{\mathrm{inc}} \rangle$ given in Equations (8) and (10) in Equation (11) and comparing the corresponding coefficients of W_{laser},

$$P_1 = P_0 Q_{\mathrm{fl}} \frac{\sigma n_g^0}{\pi (d/2)^2 h\nu} \left[1 - \exp\left\{ -2 \frac{(d/2)^2}{w_0^2} \right\} \right]. \tag{14}$$

$$P_2 = \frac{\sigma}{\pi (d/2)^2 h\nu \gamma_{\mathrm{e}}} \left[1 - \exp\left\{ -2 \frac{(d/2)^2}{w_0^2} \right\} \right] \times \left(1 + \frac{\gamma_{\mathrm{e}}^{\mathrm{ic}}}{\gamma^{\mathrm{tr}} + \gamma_{\mathrm{t}}^{\mathrm{ic}}} \right). \tag{15}$$

From the coefficient P_1, describing the linear dependence of the signal on the laser power W_{laser} and given in Equation (14), the number of fluorochromes n_g^0 can be calculated

$$n_g^0 = P_1 \frac{1}{P_0} \frac{1}{Q_{\mathrm{fl}} \sigma} \frac{\pi (d/2)^2 h\nu}{\left[1 - \exp\left\{ -2 \frac{(d/2)^2}{w_0^2} \right\} \right]}. \tag{16}$$

Alternatively, by combining Equations (14) and (15) the additional information of the coefficient P_2—accounting for the nonlinearity or saturation—is exploited and the number of molecules in the ground state is given by

$$n_g^0 = \frac{P_1}{P_2} \frac{1}{P_0} \frac{1}{Q_{\mathrm{fl}} \gamma_{\mathrm{e}}} \left(1 + \frac{\gamma_{\mathrm{e}}^{\mathrm{ic}}}{\gamma^{\mathrm{tr}} + \gamma_{\mathrm{t}}^{\mathrm{ic}}} \right). \tag{17}$$

When applying Equation (16) to derive n_g^0, the beam waist of the laser w_0, the particle area, photon energy and the absorption cross-section of the fluorochrome have to be known. These quantities do not enter Equation (17), instead the knowledge of the relaxation rates γ_{e}, $\gamma_{\mathrm{e}}^{\mathrm{ic}}$, γ^{tr}, and $\gamma_{\mathrm{t}}^{\mathrm{ic}}$ is required. On the other hand, if the characterization of the fluorophore is needed, the ratio $\gamma_{\mathrm{e}}^{\mathrm{ic}}/(\gamma^{\mathrm{tr}} + \gamma_{\mathrm{t}}^{\mathrm{ic}})$ of relaxation rates concerning the intercombination transitions $|e\rangle \rightarrow |t\rangle$ and $|t\rangle \rightarrow |g\rangle$ can be deduced from the experiments by simply converting Equation (15) to

$$\frac{\gamma_{\mathrm{e}}^{\mathrm{ic}}}{\gamma^{\mathrm{tr}} + \gamma_{\mathrm{t}}^{\mathrm{ic}}} = \left(P_2 \frac{\gamma_e}{\sigma} \frac{\pi (d/2)^2 h\nu}{\left[1 - \exp\left\{ -2 \frac{(d/2)^2}{w_0^2} \right\} \right]} \right) - 1. \tag{18}$$

We analyzed our experimental data presented in Fig. 2 by fitting the parameters P_1 and P_2 using Equation (12), their values are given in Table I and the resulting curve is included in Fig. 2. As was pointed out by R. Y. Tsien and A. Waggoner [19], the triplet lifetime is extremely sensitive against the environment of FITC. Hence we used Equation (16) to derive the number n_{g}^0 of molecules bound to the polystyrene bead and calculated the triplet lifetime $1/\gamma_{\mathrm{t}}^{\mathrm{ic}}$ from Equation (18). The values for n_{g}^0 and $\gamma_{\mathrm{t}}^{\mathrm{ic}}$ obtained from the model are included in Table I together with all necessary input values, which were taken from reference [19] or derived from experimental conditions. The number of molecules derived from the rate equation model amounts to $n_{\mathrm{g}}^0 = 29000 \pm 3000$. The uncertainty of about 10% given for n_{g}^0 is mainly caused by the uncertainty of P_0, i.e. the transmission and conversion efficiency of the optical detection system. The rate equation model is expected to give the correct number of molecules, provided the approximations are adequate and the photo-physical properties of the bound fluorophore are inserted in the equations. However, these quantities are not available and we used the values for fluorescein in solution. According to Equation (16), the calculated number is inversely proportional to the quantum efficiency Q_{fl}. Since the quantum efficiency will presumably be reduced upon binding, the value for n_{g}^0 represents a lower limit. For the ratio $\gamma_{\mathrm{e}}^{\mathrm{ic}}/(\gamma^{\mathrm{tr}} + \gamma_{\mathrm{t}}^{\mathrm{ic}})$ of relaxation rates (see Equation (18)) we obtain a lower limit, too, because the excited state relaxation rate γ_{e} is expected to increase due to additional relaxation channels when bound to microspheres.

Future efforts aim at the validation of the rate equation model discussed, e.g. by comparing the calculated values for the number of molecules with MESF units for various fluorophores. In addition, quantification of fluorescence by analyzing its saturation behavior, demonstrated for an ensemble of microbeads, can be extended to single particles by simply focussing a second laser beam into the flow cell of the cytometer. Thus, the

Table I. Summary of Symbols, Definitions and Values used to Analyze the Saturation of Laser-Induced Fluorescence of Fluorescein Stained Beads

Symbol	Definition	Numerical value	Unit
P_0	Total conversion efficiency of light detection system	9.81×10^{-14}	V s
P_1	Fit parameter describing the linear dependence of fluorescence intensity on n_g^0	**3.45**	V/W
P_2	Fit parameter accounting for the nonlinearity of laser induced fluorescence	**15.0**	W
w_0	Laser beam waist radius	5	μm
$h\nu$	Photon energy	4.07×10^{-19}	J
d	Diameter of sphere	6.1	μm
Q_{fl}	Quantum efficiency for fluorescence emission	0.9	1
n_{g}^0	Number of fluorescence molecules in the ground state when entering the laser beam	$\mathbf{2.9 \times 10^4}$	1
σ	Absorption cross-section at 488 nm	3.06×10^{-8}	$\mu\mathrm{m}^2$
γ^{tr}	Relaxation rate due to transit time	5×10^5	s^{-1}
γ_{e}	Total relaxation rate of excited state	2.22×10^8	s^{-1}
$\gamma_{\mathrm{e}}^{\mathrm{ic}}$	Relaxation rate of excited state due to intercombination	6.66×10^6	s^{-1}
$\gamma_{\mathrm{t}}^{\mathrm{ic}}$	Relaxation rate of triplet state due to intercombination	$\mathbf{4 \times 10^6}$	s^{-1}
$\gamma_{\mathrm{e}}^{\mathrm{ic}}/(\gamma^{\mathrm{tr}} + \gamma_{\mathrm{t}}^{\mathrm{ic}})$	Ratio of relaxation rates	**1.48**	1

Note. Values for the fit parameters and values derived from the rate equation model are given in bold type.

fluorescence of the same particle can be measured further downstream in a second interaction region using different irradiances for both laser beams to determine saturation. Moreover, quantification of photobleaching, which was not considered in our rate equation approach, is accessible by measuring the fluorescence of a single particle twice, preferable using identical irradiances for both laser beams. Observation of fluorescence saturation of single particles is of particular interest when analyzing cells, since the variation of fluorescence intensity of defined (sub-) populations is considerably larger compared to fluorescent beads. Saturation behavior, derived from the relative signals observed in the first and second laser beams, can be used to select (living) cells of interest for subsequent flow cytometric sorting and detailed microscopic investigation including quantification of fluorescence by single molecule bleaching.

Microscopic Single Molecule Bleaching of Immobilized Fluorophores

To fully exploit the potential of the rate equation model described above, it is necessary to determine the photo physical properties of the fluorophore when coupled to beads or to cells using labeled monoclonal antibodies. Besides the strong dependence of the triplet lifetime on the environment, e.g. the oxygen concentration [19], the lifetime of the excited state and the fluorescence quantum efficiency might be affected as well. In the following, we show that high sensitivity microscopy can be used to yield the information required. By this means, traceability of flow cytometric quantification of fluorescence is possible. For demonstration, we observed the fluorescence of Alexa 647 fluorochromes bound to an immobilized streptavidin molecule, the results are shown in Fig. 4. The image size amounts to 10 μm by 10 μm and the fluorescence intensity is proportional to the count rate. Seven diffraction limited spots with Gaussian distributions of fluorescence intensity are clearly visible, the corresponding number of fluorescent molecules are included in the figure. For validation, we moved the laser focus to several of the fluorescence spots and determined the temporal dependence of the fluorescence intensity. In Fig. 5, a typical result of these measurements is depicted, the laser was tuned at the position in Fig. 4 corresponding to the largest signal. Compared to the power used to record the image depicted in Fig. 4, we reduced the power of the exciting laser by a factor of 25 to observe the fluorescence signals for a longer time. At first, the laser is turned off to identify the background count rate of approximately 100 counts per second. When switching on the laser, the count rate shortly increased to 900 Hz and dropped to about 500 Hz for 15 s. Again, at a time of 28 s the observed count rate decreased, remained constant until 85 s, and finally drop to the starting value. This stepwise reduction of fluorescence intensity is interpreted as bleaching of single molecules, each Alexa 647 molecule caused a fluorescent signal of about 200 counts/s. The count rates indicated by horizontal lines in Fig. 5, correspond to the fluorescence of four, two and one Alexa 647 molecules and the background fluorescence, respectively.

Microscopic fluorescence bleaching is expected to allow the determination of the number of fluorescent molecules bound to a bead or a cell. First, the decrease of fluorescence intensity integrated over the volume of the particle has to be measured and extrapolated to the initial point of the measurement, i.e. to zero time. After sufficient bleaching, when the remaining number of

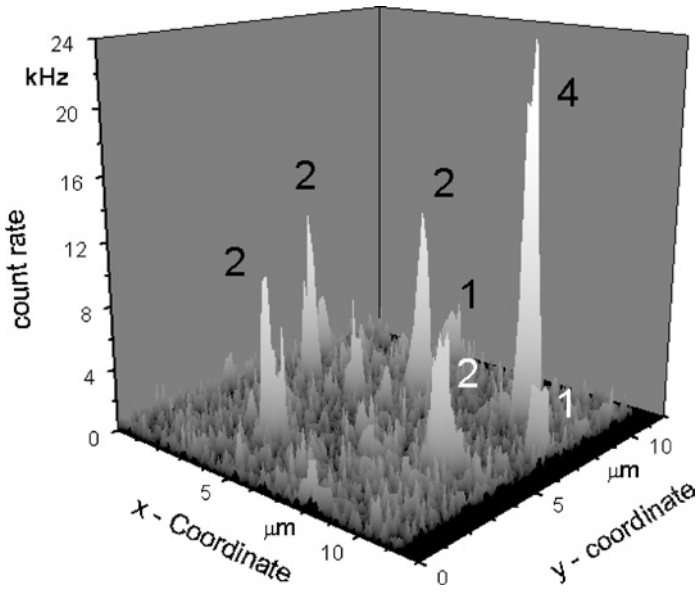

Fig. 4. Confocal microscopic image (10 μm by 10 μm) of laser induced fluorescence of single streptavidin Alexa 647 complexes immobilized on a cover glass appearing as diffraction limited spots. We have included in the depiction the number of Alexa 647 fluorochromes bound to each of the streptavidin molecules.

fluorochromes is low enough, stepwise single molecule bleaching can be observed. This procedure allows normalization or traceability of fluorescence to molecules exposed to the environment occurring when bound to cells or microparticles.

SUMMARY AND PERSPECTIVES

We demonstrated that saturation of laser induced fluorescence in a flow cytometer is feasible to calculate the number of fluorochromes bound to a microbead or to a

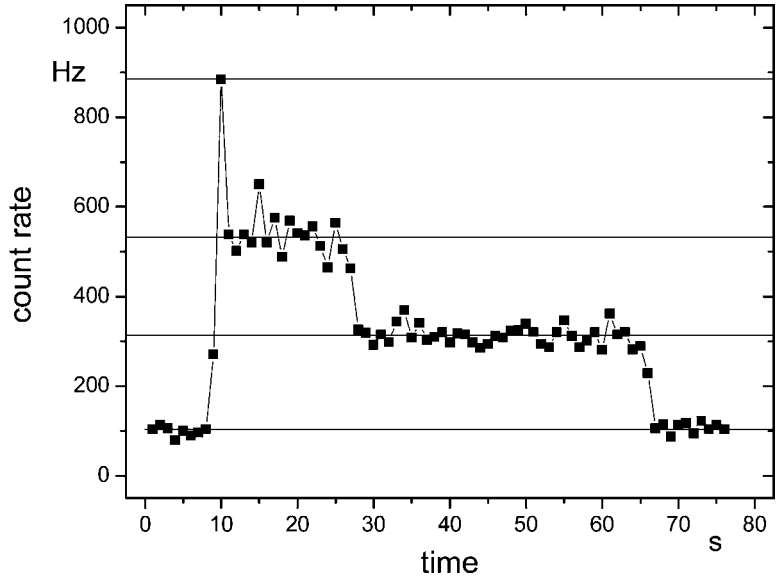

Fig. 5. Time dependence of laser induced fluorescence of an streptavidin alexa 647 complex exhibiting stepwise bleaching of single fluorophores. The complex of highest intensity in Fig. 5 was chosen by tuning the position of the laser focus to the corresponding coordinates.

cell via fluorescently labeled antibodies. In addition, the ratio of intersystem crossing rates from the excited in the triplet and from the triplet in the ground state follows from saturation measurements and analysis by the rate equation model presented in this paper. To ensure that the excited state lifetime or the total relaxation rate of the excited state for the bound fluorochromes are available instead of values valid for free fluorochromes, it would be necessary to combine flow cytometric saturation measurements and flow cytometric lifetime measurements [21,22].

Flow cytometry also features the potential to apply the saturation technique to single particle investigation, which is of particular interest when studying biological samples. Whereas stained microbeads possesses a narrow distribution of fluorescence intensity and average values of the ensemble is representative for individual beads, cells belonging to the same population might exhibit a broad range of fluorescence signals. To select single cells according to their number of fluorophores by flow cytometric sorting, the setup has to be supplemented to allow the interaction of each cell with two laser beams of different, properly chosen irradiances.

To ensure traceability of the results obtained by flow cytometric saturation experiments, microscopic bleaching of fluorescence of microbeads or stained cells is suited. Besides successive bleaching of fluorescence the procedure of microscopic quantification has to include integration over the particle volume and extrapolation to the number of fluorophores at the beginning of the measurement. Finally, as we demonstrated in this paper, stepwise single molecule bleaching serves to obtain the specific *in situ* fluorescence intensity of a single fluorophore thus allowing to derive the total amount of fluorescent molecules. Fluorescent particles, characterized by such a procedure, could be used to determine the instrument specific sensitivity (i.e. P_0) of the corresponding fluorescence detection channel of flow cytometers.

REFERENCES

1. H. M. Shapiro (2003). *Practical Flow Cytometry*, 4th ed., Wiley, Hoboken, New Jersey.
2. M. R. Melamed, T. Lindmo, and M. L. Mendelsohn (1990). *Flow Cytometry and Sorting*, 2nd ed., Wiley, New York.
3. O. D. Laerum and R. Bjerknes (1992). *Flow Cytometry in Hematology*, Academic Press, London.
4. A. Radbruch (1992). *Flow Cytometry and Cell Sorting*, Springer-Verlag, Berlin.
5. A. L. Landay, K. A. Ault, K. D. Bauer, and P. S. Rabinovitch (1993). *Clinical Flow Cytomery*, New York Academy of Sciences, New York.
6. M. G. Ormerod (1994). *Flow Cytometry, A Practical Approach*, 2nd ed., Oxford University Press, New York.
7. R. C. Braylan, M. J. Borowitz, B. H. Davis, G. T. Stelzer, and C. C. Stewart (1997). U.S.-Canadian consensus recommendations on the immunophenotypic analysis of hematologic neoplasia by flow cytometry, *Cytometry* **30**, 213.
8. C. D. Jennings and K. A. Foon (1997). Recent advances in flow cytometry: Application to the diagnosis of hematologic malignancy, *Blood* **90**, 2863–2892
9. G. Rothe and G. Schmitz (1996). Consensus protocol for the flow cytometric immunophenotyping of hematopoietic malignancies, Working Group on Flow Cytometry and Image Analysis, *Leukemia* **10**, 877–895
10. R. L. Hengel and J. K. Nichlson (2001). An update on the use of flow cytometry in HIV infection and AIDS, *Clin. Lab. Med.* **21**, 841–856.
11. D. Campana and E. Coustan-Smith (2004). Minimal residual disease studies by flow cytometry in acute leukemia, *Acta Haematol.* **112**, 8–15.
12. A. Scheffold and A. Thiel (2004). Detection of antigen-specific lymphocytes, *J. Lab. Med.* **28**(4), 299–306.
13. J.-C. Strohmeyer, C. Blume, C. Meisel, W.-D. Doecke, M. Hummel, C. Hoeflich, K. Thiele, A. Unbehaun, R. Hetzer and H.-D. Volk (2003). Standardized immune monitoring for the prediction on infections after cardiopulmonary bypass surgery in risk patients, *Cytometry* **53B**, 54–62.
14. S. B. Iyer, M. J. E. Bishop, B. Abrams, V. C. Maino, A. J. Ward, T. P. Christian, K. A. Davis, QuantiBRITE^{TM}: A new standard for fluorescence quantification, www.bdbiosciences.com/immunocytometry_systems (see literature, White Papers, QuantiBRITE^{TM} White Paper).
15. Y. Gerena-López, J. Nolan, L. Wang, A. Gaigalas, A. Schwartz, and E. Fernández-Repollet (2004). Quantification of EGFP Expression on Molt-4 T cells using calibration standards, *Cytometry* **60A**, 21–28.
16. A. Schwartz, L. Wang, E. Early, A. Gaigalas, Y.-Z. Zhang, G. E. Marti, and R. F. Vogt (2002). Quantitating Fluorescence Intensity From Fluorophore: The Definition of MESF Assignment, *J. Res. Natl. Inst. Stand. Technol.* **107**(1), 83–91.
17. V. Ost, J. Neukammer, and H. Rinneberg (1998). Flow cytometric differentiation of erythrocytes and leucocytes in dilute whole blood by light scattering, *Cytometry* **32**, 191–197.
18. A. S. Waggoner (1990). Fluorescent probes for flow cytometry, in M. R. Melamed, T. Lindmo, and M. L. Mendelsohn (Eds.), *Flow Cytometry and Sorting*, Wiley-Liss, New York, pp. 209–225.
19. R. Y. Tsien and A. Waggoner (1995). Fluorophores for confocal microscopy, in J. B. Pawley (Ed.), *Handbook of Biological Confocal Microscopy*, 2nd ed., Plenum Press, New York, pp. 267–279.
20. R. A. Mathies and L. Stryer (1986). Single-molecule fluorescence detection: A feasibility study using phycoerythrin, in L. Taylor, A. Waggoner, R. Murphy, F. Lanni, and R. Birge (Eds.), *Applications of Fluorescence in the Biomedical Science*, Alan Liss, New York, pp. 129–140.
21. B. G. Pinsky, J. J. Ladasky, J. R. Lakowicz, K. Berndt, and R. A. Hoffman (1993), Phase-resolved fluorescence lifetime measurements for flow cytometry, *Cytometry* **14**, 123–135.
22. J. A. Steinkamp and H. A. Crissman (1993). Resolution of fluorescence signals from cells labeled with fluorochromes having different lifetimes by phase-sensitive flow cytometry, *Cytometry* **14**, 210–216.